Int. J. Heat Mass Transfer. Vol. 36, No. 18, pp. 4433–4441, 1993
Printed in Great Britain

0017-9310/93 $6.00 + 0.00

Thermal hysteresis in fibrous insulation

C. J. SIMONSON, Y.-X. TAO and R. W. BESANT
Department of Mechanical Engineering, University of Saskatchewan, Saskatoon, Saskatchewan S7N 0W0, Canada

(*Received* 28 *January* 1993 *and in final form* 13 *May* 1993)

Abstract—Thermal hysteresis, characterized by both the difference between the adsorption and desorption isotherms and the difference between heat of adsorption and heat of desorption, is investigated for typical fiberglass insulation. The heats of sorption are measured, as a function of equilibrium adsorbate mass, using an apparatus based on the energy balance principle. A numerical simulation, employing a local-volume-averaging formulation and measured heats of sorption, is performed to examine the effect of thermal hysteresis on simultaneous heat and mass transfer and moisture/frost accumulation in a transient process for a fiberglass insulation slab. The results show that the thermal hysteresis effect is pronounced regardless of whether an insulation slab is initially dry or wet. Neglecting hysteresis effects in simulating a dynamic transport process can lead to errors in the instantaneous heat flux of up to 51% for an initially dry fiberglass slab and 23% for an initially moist slab.

1. INTRODUCTION

MOISTURE problems in building envelopes have been long recognized by practitioners and building code officials. While various means have been proposed for moisture control strategies for building envelopes [1], researchers have been developing analytical and numerical tools to evaluate moisture control improvements, especially taking into account the interactions between various building components under coupled heat and mass transfer. Recent developments include simulation of dynamic processes of coupled heat transfer, vapor diffusion, air or liquid movement and phase change within exterior walls and roof structures [1–4]. For validation, such simulation models need rigorous analyses, especially for identifying the significance of each individual physical effect. This cannot be accomplished without experimental studies.

One of the most important wall components related to moisture problems and energy conservation is thermal insulation. It is known that for a typical wall configuration with a wall cavity filled with porous insulation (e.g. fiberglass) moisture or frost accumulation occurs in several forms: condensation or frosting between the permeable insulation and low-permeable wall component, adsorption of water vapor within the fiberglass insulation [5–7], and absorption, wicking and diffusion of moisture within the wood frame and sheathing members. The transport mechanisms causing moisture accumulation include vapor diffusion and pressure-driven airflow through porous components [8].

In this study, we are concerned with moisture movement within the fibrous insulation and on the boundaries that occurs much more rapidly than moisture movement through the wood frame and sheathing members. Because the mass of vapor adsorbed onto the glass fibers inside the insulation is small compared to that adsorbed onto the adjacent low-permeable surface of the wall, it is often neglected. However, experimental evidence [7] shows that thermal energy exchange between the adsorbed phase and surrounding phases during an adsorption (or desorption) process is pronounced and can alter the local temperature significantly. The adsorption and desorption processes defined in this context are the mass transfer processes with the local relative humidity in fibrous insulation being less than 100%. It has been pointed out that such adsorption or desorption effects could lead to a cumulative impact on the distributions of temperature and moisture for the insulation (and the wall assembly) undergoing diurnal changes. However, the studies by Tao *et al.* [7, 9] have not addressed the issue of combined adsorption and desorption effects (i.e. hysteresis) in a transient heat and mass transport process.

Commercial fiberglass insulation (batts or loose fills) has a different equilibrium adsorbate mass exposed to air at a particular temperature and humidity after undergoing an adsorption or desorption process. This mass sorption hysteresis phenomenon is characterized by two different isotherms (the relation between the equilibrium adsorbate mass and partial pressure, or relative humidity, of the adsorptive gas) and is also accompanied by two different energy exchange capacities or heats of adsorption and desorption. Physically the hystereses in mass transfer and heat transfer occur concurrently; mass transfer could be measured separately but the heats of sorption measurement requires both heat and mass transfer data. Therefore, in this paper, we combine the hysteresis in mass transfer and heat transfer into a so-called 'thermal hysteresis' phenomenon. We first define this physical phenomenon, then present an experimental investigation, using a flow calorimeter, to measure the heats of adsorption and desorption,

NOMENCLATURE

C	empirical constant in equations (1) and (2)
c_p	heat capacity at constant pressure [J kg^{-1} K^{-1}]
D_{eff}	effective vapor diffusivity [m^2 s^{-1}]
Fo	Fourier number, $\alpha_{eff}t/L^2$
h_a	heat transfer coefficient [J m^{-2} s^{-1} K^{-1}]
h_m	mass transfer coefficient [m s^{-1}]
h'	ratio of the enthalpy (heat) of sorption to the enthalpy of vaporization
Δh	enthalpy of phase change [J kg^{-1}]
k	thermal conductivity [J m^{-1} s^{-1} K^{-1}]
L	thickness of the insulation [m]
m	total mass of the dry insulation [kg]
$\dot{m}$	rate of phase change [kg m^{-3} s^{-1}]
p	pressure [Pa]
Q'	heat flux ratio
R_v	vapor gas constant [J kg^{-1} K^{-1}]
t	time [s]
T	temperature [K]
W	percentage water content by weight [%]
z	coordinate axis [m].

Greek symbols

α	thermal diffusivity [m^2 s^{-1}]
ε	volume fraction
ρ	density [kg m^{-3}]
ϕ	relative humidity.

Subscripts

a	air
c	cold
s	saturated
t	total
tr	transition
v	vapor phase
β	liquid or ice phase
γ	gas phase which consists of air and water vapor
σ	solid phase
∞	ambient
0	initial.

and finally, analyze the significance of thermal hystersis effects on a dynamic heat and mass transport process in porous insulation through a numerical simulation, which incorporates the experimental findings. To emphasize the effect of thermal hysteresis, air infiltration is not included in the simulation.

2. THERMAL HYSTERESIS

The hysteresis in equilibrium mass of adsorbate for fiberglass materials has been indicated by several experimental studies, as summarized in ref. [7]. From these data sets, it can be reasonably assumed that for a medium-dry-density fiberglass batt, the adsorption isotherm exhibits a trend that can be approximated by the Brunauer–Emmett–Teller (BET) equation,

$$W/W_m = \frac{C\phi}{[1-\phi][1+(C-1)\phi]}, \quad (1)$$

while the desorption isotherm follows the Langmuir equation

$$W/W_m = \frac{C\phi}{1+C\phi}, \quad (2)$$

where W_m and C are empirical constants and $W = \varepsilon_\beta(\rho_\beta/\rho_0)$.

Figure 1 shows a typical hysteresis loop of adsorption and desorption isotherms for fiberglass insulation. For a given relative humidity ($0 < \phi < 90\%$), the equilibrium mass for adsorption is smaller than that for desorption. This is primarily due to capillary effects that arise in porous materials with a large pore-size distribution [10]. Fiberglass insulation has a significant pore size variation due to a somewhat random distribution of fibers. Compared to other hygroscopic materials, the magnitude of adsorbate mass in fiberglass insulation is much smaller, but this does not prevent fiberglass insulation from exhibiting strong thermal hysteresis effects.

The physical adsorption of a gas on a surface is accompanied by the release of thermal energy; conversely, the physical desorption of a gas from a solid surface requires the addition of thermal energy. These heats of sorption are defined by the initial and final thermodynamic states of the system and the conditions under which any heat flux takes place; examples are adiabatic heat of sorption, isosteric heat of sorption, etc. [10]. In engineering related problems the most common sorption process is isosteric. In

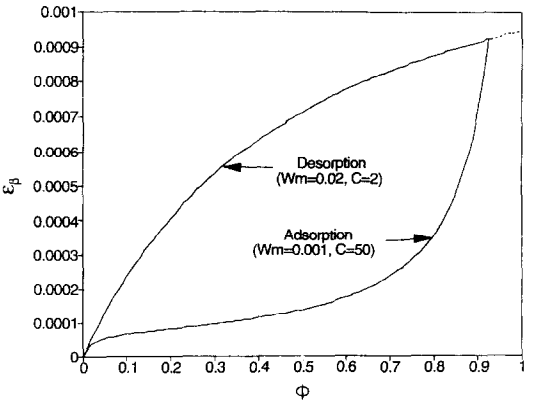

FIG. 1. Typical adsorption and desorption isotherms for fiberglass insulation [6, 10].

thermodynamic terms, the isosteric heat of sorption is the differential enthalpy of sorption that can be used in solving the differential energy equation. In general, the isosteric heat of sorption at a given ambient pressure has the following functional form,

$$h_{sorp} = f(W, T, \text{adsorptive gas, adsorbent solid}). \tag{3}$$

Because the equilibrium content of adsorbate, W, is a function of temperature, T, and relative humidity, ϕ, for a given sorptive–sorbent system, equation (3) can be written as,

$$h_{sorp} = f(\phi, T). \tag{4}$$

3. EXPERIMENT

A simple and practical method developed by Tao *et al.* [9] is used to measure both heat of adsorption and heat of desorption for a typical, medium-density fiberglass slab. This method is based on the same principles used in designing a flow calorimeter. The control volume, shown in Fig. 2, consists of an insulation matrix that undergoes an adsorption or desorption process. Initially the control volume that contains the insulation test sample is at a uniform temperature, T_0, and relative humidity, ϕ_0. At time $t = 0^+$, air at a controlled temperature, T_∞, and humidity, ϕ_∞, flows through the sample. To minimize any heat fluxes, except due to sorption within the test sample, T_0 is set to be equal to T_∞ or T_1. As the air passes through the sample, adsorption or desorption takes place. This causes the air temperature leaving the control volume (T2) to change relative to the inlet temperature (T1) (Fig. 3). In the case of adsorption, thermal energy is released to the air that is passing through the test sample at a controlled rate therefore temperature (T2) rises, while for desorption this temperature decreases. When the adsorption/desorption process is completed the test sample is again in thermodynamic equilibrium with the surroundings at T_∞ and ϕ_∞. Applying the first law of thermodynamics and conservation of mass for a constant mass flow rate ($\dot{m}_a$) and a constant specific heat of air (c_{pa}), the average heat of adsorption/desorption is [9],

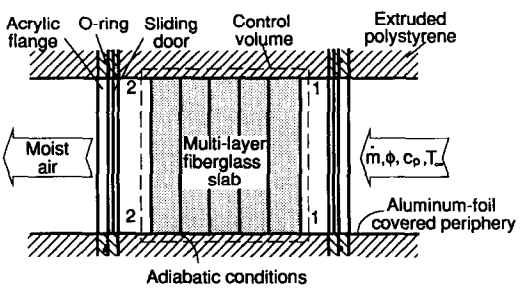

FIG. 2. The test section. Indicated also is the control volume for the derivation of the measurement principle.

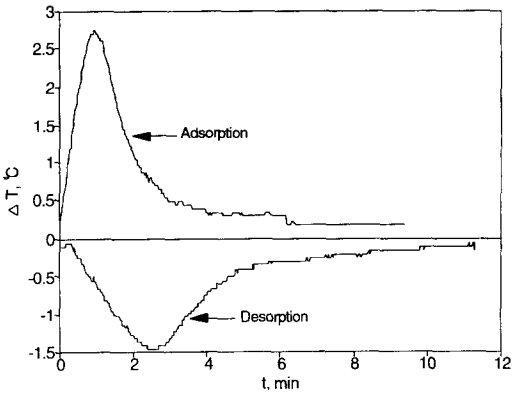

FIG. 3. Typical time variation of the experimental temperature difference $\Delta T = T_2 - T_1$ for $\rho = 71.2$ km m^{-3}.

$$\bar{h}_{sorp} = \frac{c_{pa}\dot{m}_a S}{\Delta m}, \tag{5}$$

where $\bar{h}_{sorp}$ is the average heat of adsorption/desorption, Δm is the mass of water vapor adsorbed/desorbed and

$$S = \int_0^t (T_2 - T_1)\,\mathrm{d}t \tag{6}$$

is the temperature signature (Fig. 3) and is determined using numerical trapezoidal integration.

It should be noted that the average heat of sorption, as in equation (5), from some initial state temperature, T_∞, and relative humidity, ϕ_0, to a final state of T_∞ and ϕ_∞ is not the same as the heat released/absorbed at any intermediate state. To get the thermodynamic state heat of adsorption/desorption, we can write the average heat of adsorption/desorption as a function of adsorbed/desorbed water vapor, W, by choosing a proper correlation,

$$\bar{h}_{sorp} = f(W, T_\infty), \tag{7}$$

so that for a given T_∞ we can write the thermodynamic heat of sorption as

$$h_{sorp}(W) = \frac{\partial W \bar{h}_{sorp}}{\partial W} = \bar{h}_{sorp} + W\frac{\partial \bar{h}_{sorp}}{\partial W}, \tag{8}$$

where, by definition

$$\bar{h}_{sorp} = \frac{1}{W}\int_0^W h_{sorp}\,\mathrm{d}W. \tag{9}$$

From a thermodynamic point of view, the above-defined average heat of sorption has a reference point at zero vapor pressure corresponding to a zero relative humidity. This condition is very difficult to be controlled by the present experiment. Besides, this absolute dry condition is never met in service. In this study, all the measured data for W and h' are based on the reference state of T_∞ and $2 < \phi < 4\%$. For slight variations in the reference state, we need only to use a transformation of $W = W^* - W_0$ where W^* is the absolute mass of adsorbate with respect to the vacuum

state and W_0 is the residual mass of adsorbate at $0 < \phi < 5\%$ such that equations (8) and (9) are still the valid representations of the heats of sorption for practical situations. Therefore, from the measured average heat of sorption (equation (5)), the thermodynamic state heat of sorption can be found using equation (8). For comparison with heat of vaporization, the results will be presented as a ratio of the heat of adsorption/desorption to heat of evaporation. That is,

$$h' = \frac{h_{\text{sorp}}}{h_{\text{fg}}} \quad \text{or} \quad \bar{h}' = \frac{\bar{h}_{\text{sorp}}}{h_{\text{fg}}}, \tag{10}$$

where h' refers to the latent heat ratio and h_{fg} is the heat of evaporation.

The schematic of the apparatus is shown in Fig. 4. The apparatus and test procedure for adsorption are discussed in ref. [9]. The insulation sample is initially dry and the air is moist for adsorption; whereas, the sample is initially moist and the air is dry for desorption. For adsorption, the insulation sample is first dried with dry air from a desiccant air loop; whereas, for desorption the insulation is humidified with air from an air bath loop. After the initial thermal and mass equilibrium condition is reached, the sample is weighed. The test begins by opening the upstream and downstream sliding doors (see Fig. 2) and using the vacuum pump to draw air through the sample (see Fig. 4). In the adsorption test, the moist air is drawn from the environment chamber, and in the desorption test, the dry air is drawn from a large plastic bag filled with dry air at ambient pressure. The air in the plastic bag is dried with a desiccant drying loop that can provide air at relative humidities below 5%. The mass flow rate of air is measured with the orifice plate and the computer data acquisition unit continuously records the temperature of all three thermocouples. The typical airflow rate is measured at 2.44×10^{-3} kg s^{-1}. Initially the temperature at the downstream thermocouple (TC2), shown in Fig. 4, changes as sorption occurs. When the temperature of TC2 returns to that of TC1, the equilibrium is accomplished and the test is stopped. The final mass of the sample is then measured and the average heat of sorption is found using equation (5). Because the final equilibrium relative humidity (i.e. the reference point) in a desorption test is higher than the initial relative humidity for an adsorption test, the sample after the desorption test is further dried to match the same reference point as that for the adsorption tests. The equilibrium water content for the desorption test is then corrected based on the drying results.

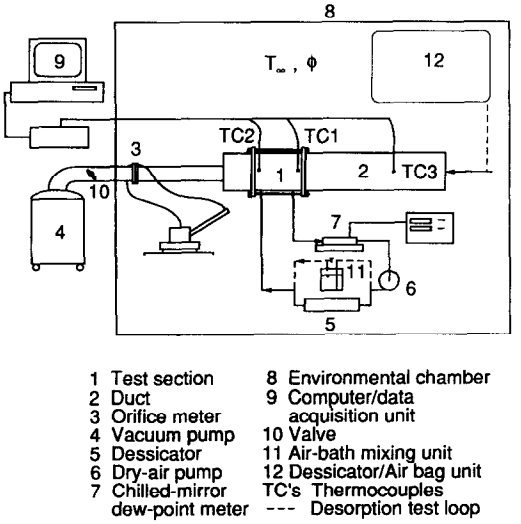

FIG. 4. The schematic of the apparatus.

The fiberglass samples used in this study have a dry density ranging from 54.3 to 71.2 kg m^{-3}, percentage of the bonding material about 6.7 to 7.8 and the average fiber diameter of 10 μm. These data were obtained from at least four data points measured in our laboratory. The overall system error for measured heat of sorption is 10% and the random error or repeatability is normally within $\pm 15\%$. The main source of error comes from the measurement of Δm ($\pm 10\%$). Increasing the ratio of Δm to the total sample mass should reduce this error [9], but this improvement is limited by the choice of a proper weighing scale and size of the apparatus.

4. HEATS OF SORPTION

The measured average heats of adsorption and desorption are shown in Fig. 5, plotted as $\bar{h}'$ vs W, where W is the mass percentage of vapor adsorbed/desorbed defined as

$$W = \frac{\Delta m}{m} \times 100 \tag{11}$$

where m is the total mass of dry sample.

It can be seen that $\bar{h}'$ is always greater than unity and is larger for low W (as expected). Physically, low W values correspond to the case where only a single molecular layer is being adsorbed or desorbed from

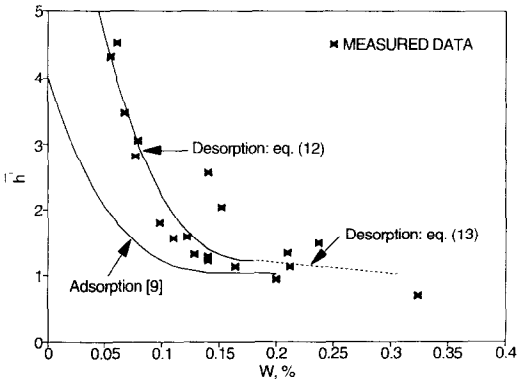

FIG. 5. The ratio of the average heats of adsorption and desorption to the heat of vaporization as a function of W, %.

the insulation fibers. The bonding forces between the fibers and the water molecules therefore prevail, and are stronger than those between water molecules; hence, more energy is needed to break the bond during desorption (and vice versa during adsorption) at low W. As the mass adsorbed/desorbed is increased there are many layers of water vapor molecules on the fiber, and as a result the bonding is basically between water molecules, resulting in a lower enthalpy of sorption.

Thermal hysteresis is evident in the average heats of adsorption and desorption shown in Fig. 5. The curves are similar in that the heats of adsorption and desorption are many times greater than the heat of vaporization for low values of W. Also, both curves approach the heat of vaporization for larger values of W. The curves are different in that the heat of desorption is always greater than the heat of adsorption and particularly for low values of W. For example, the first experimental data point for desorption is $\bar{h}' = 4.5$ for $W = 0.06\%$ which is 2.5 times that for adsorption ($\bar{h}' = 1.8$ at $W = 0.06\%$). Clearly this hysteresis effect may be significant when adsorption and desorption occur simultaneously in different regions of fiberglass insulation.

The following correlations for the average and differential heat of desorption are found by fitting a cubic polynomial to the experimental data. They are:

$$\bar{h}' = 9.218 - 118.344W + 570.428W^2 - 883.76W^3, \quad 0 \leqslant W \leqslant 0.18\%, \quad (12)$$

$$\bar{h}' = 1.58 - 1.87W, \quad 0.18 < W \leqslant 0.31\%, \quad (13)$$

$$h' = 9.218 - 236.688W + 1711.284W^2 - 3535.944W^3, \quad 0 \leqslant W \leqslant 0.052\%, \quad (14)$$

$$\bar{h}' = 1, \quad W > 0.31\%, \quad \text{and} \quad h' = 1, \quad W > 0.052\%. \quad (15)$$

These results, obtained at a temperature of 20°C, can be applied to a range from 5°C to 30°C [9]. The results in ref. [9] show that the heat of adsorption is independent of temperature in the range of 5–30°C because such a change is small on the absolute temperature scale. The same is assumed to apply to desorption. Like adsorption, the heat of desorption is independent of the porosity and permeability of the fibrous sample because the heat of desorption as defined in this paper is a specific quantity; therefore, the above correlations apply for insulation with a density of 54.3–71.2 kg m^{-3} [9].

The differential or thermodynamic state heats of adsorption and desorption are plotted together in Fig. 6. These graphs again show the thermal hysteresis effect when water vapor is adsorbed/desorbed in fiberglass insulation. Also plotted in Fig. 6 is the reported isosteric heat of desorption [7] which was derived from the desorption isotherms reported in ref. [6] (for a uniform abscissa scale a continuous curve connects the isothermal data). A large discrepancy is obvious between the measured heat of desorption and

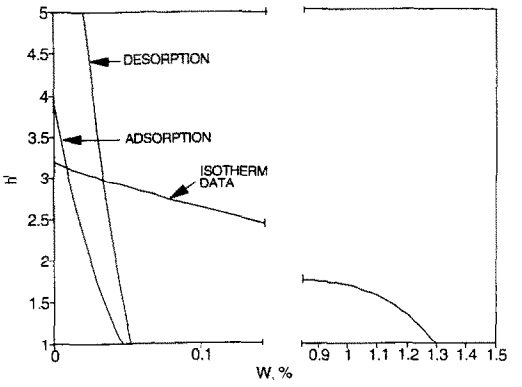

FIG. 6. Comparison of the differential heats of adsorption and desorption.

that determined from isothermal sorption data. This indicates that the only reliable way to determine the heat of adsorption/desorption for a given sorptive–sorbent system is to measure them directly with an appropriate experiment.

It should be noted that the very high heat of sorption (higher than heat of vaporization, Fig. 5) corresponds to the very low mass of sorption. This means the insulation is very dry, e.g. the local relative humidity is around 5%. This may not occur frequently in practice but it does not lead to the conclusion that adsorption and desorption processes are not important, as will be shown below.

5. NUMERICAL MODEL

Given the evidence of hysteresis phenomena in adsorption and desorption isotherms and the measured heats of adsorption and desorption, it is important to investigate the magnitude of their effect during typical transient heat and mass transfer processes in an insulation slab. A numerical study is, therefore, presented to quantify this thermal hysteresis effect.

The simultaneous heat and mass transfer problem studied is one-dimensional and transient and is formulated using the local volume averaging technique [4, 7]. Figure 7 is a schematic diagram of the physical configuration of the problem. The fiberglass slab is exposed to warm moist air on one side and a cold plate on the other. No convection (neither natural nor forced convection) from the gaseous phase is con-

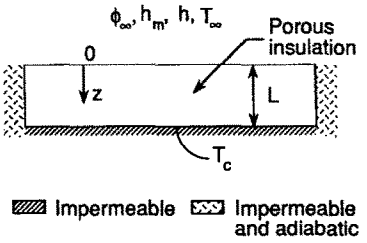

FIG. 7. Schematic diagram of an insulation slab subject to a cold plate on one side and warm moist air on the other.

sidered; therefore, vapor diffusion is the only mode for the moisture transport, and phase changes are caused by evaporation/condensation, sublimation/ablimation and adsorption/desorption. This treatment is considered to isolate the convective effects from the hygroscopic effect and to identify the significance of the hygroscopic hysteresis effect compared to bulk phase changes during moisture transport in insulation. Detailed discussions on the numerical technique used can be found elsewhere [4, 7, 11, 12]. Readers are referred to the appendix for the governing equations and initial and boundary conditions used in this study.

During adsorption and desorption the local relative humidity is below 100%, and the Clapeyron equation cannot be used to describe the relation between the vapor pressure and temperature. If we assume that the time scale required to reach sorption equilibrium at local sorption sites is of the same order as the time scale for local thermal equilibrium [7], then the sorption isotherms and the heats of sorption can be used in conjunction with the governing equations that describe a dynamic transport process. The typical sorption isotherms, shown in Fig. 1, and the appropriate differential heats of adsorption and desorption, shown in Fig. 6, are employed in the numerical calculation. It is further assumed that the relation for h' could be extrapolated to the below-freezing temperature range such that h' represents the ratio of heat of sorption to the heat of sublimation. This assumption is based on the observation that the $h'-W$ relation is not very sensitive to the absolute temperature. The formulation is then complete. It should be noted that in Fig. 1 the adsorption and desorption isotherms intersect at $\phi = 92.3\%$. In the numerical model, the desorption curve (broken line in Fig. 1) is used for both adsorption and desorption when the relative humidity is greater than 92.3%.

To avoid further complication, frost accumulation on the cold surface is not included as a special boundary condition even though experimental evidence shows it to be important [13].

6. NUMERICAL RESULTS

In this study two cases are examined using the physical model in Fig. 7: case 1 where dry insulation undergoes wetting and case 2 where an initially moist insulation slab is being dried. In case 1, the insulation is initially dry ($\phi_0 = 10^{-7}$) and at room temperature, T_∞, when it is subject to very moist air ($\phi_\infty = 0.97$) on the warm side ($z = 0$) and a cold plate (T_c) at $z = L$. During this process, adsorption is the dominant mode for local phase change for a large portion of the insulation slab, and due to the initially low moisture content of the insulation thermal hysteresis effects are expected to be significant during the transient period. For case 2, the slab initially contains room temperature air at a high local relative humidity ($\phi_0 = 0.8$) when it is exposed to a lower ambient relative humidity ($\phi_\infty = 0.4$) on the warm side ($z = 0$) and temperature, T_c, at $z = L$. In this case desorption prevails at the places near the warm side of the slab but, due to the high moisture content of the insulation, the heats of adsorption and desorption nearly equal the heat of evaporation or sublimation. The effect of the cold plate temperature is addressed by testing both cases for cold plate temperatures well below freezing, 252 K, and slightly above freezing, 278 K.

A transition Fourier number (Fo_{tr}) can be used to characterize the hygroscopic effects of a fiberglass insulation [7] and is defined as the dimensionless time when the local air relative humidity at $z/L = 0.9$ is greater than 90%. The transition Fourier number characterizes the commencement of the quasi-steady state in which hygroscopic effects are negligible although capillary effects are still present. Figure 8(a) shows Fo_{tr} for cases 1 and 2 when the plate temperature is 252 K. It is observed that Fo_{tr} for an initially dry slab, is much larger than that for an initially wet slab. In Fig. 8(b), the results for $T_c = 278$ K (i.e. no frosting effects) are shown. In this case, Fo_{tr} is slightly larger than that for a sub-freezing cold plate temperature. The results for which no hygroscopic, thermal hysteresis effects are used are also shown as the broken lines in Fig. 8. For no hysteresis effects, only one of the sorption isotherms and one of the heats of sorption are used. The desorption isotherm (2) is used in case 1 where adsorption is expected to predominate, and the adsorption isotherm (1) is used

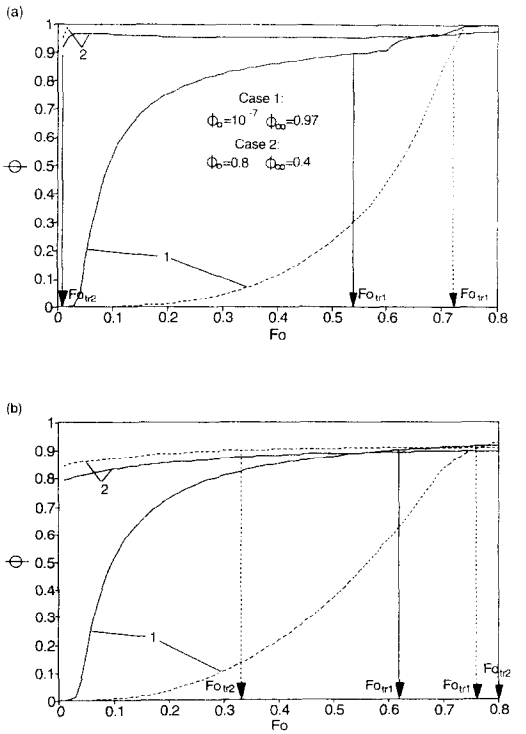

FIG. 8. Time variation of the local relative humidity at $z = 0.9$ indicating a transition Fourier number for (a) $T_c = 252$ K and (b) $T_c = 278$ K. The broken lines correspond to the results assuming no thermal hysteresis effects.

in case 2 where desorption should prevail. The heat of desorption is used for case 1 but the heat of adsorption for case 2. These selections are made to illustrate the consequence of neglecting thermal hysteresis effects in modeling typical drying or wetting processes. Figure 8 shows very different results when hysteresis effects are altered for the initially dry sample, case 1, by using only the desorption isotherm equation (2) in place of the adsorption isotherm (1). The relative humidity curves for air in Fig. 8 for case 1 closely resemble the adsorption and desorption volume fraction curves in Fig. 1. This indicates that this process is dominated by molecular diffusion in the interstitial space of the fibrous insulation and the hygroscopic adsorption process up to the transition Fourier numbers, Fo_{tr}.

The effect of the cold plate temperature in Figs. 8(a) and (b) does not cause much change in the air relative humidity for the case of the initially dry sample (case 1) but it does have a large effect on Fo_{tr} for case 2 with an initially moist fiberglass slab. In Fig. 8(b), Fo_{tr} at 0.8 corresponds to a 3.56 h hygroscopic period for the problem under investigation. A hygroscopic time period this large would imply that steady state conditions may not exist in typical fibrous insulation systems used in many building envelopes subject to large diurnal variations in temperature and humidity.

Figure 9 shows a heat-flux ratio Q' as a function of Fo. This heat transfer ratio is defined at the cold side of the insulation as the ratio of heat flux for the specified dynamic process to that for a completely dry slab under the same temperature boundary conditions; i.e. $Q' = (k_{\text{eff}}\partial T/\partial z)_{z=L}/(k_{\text{dry}}\partial T/\partial z)_{z=L,\text{dry}}$. Once again, the broken lines in Fig. 9 are for the case where the hysteresis effects are neglected using the assumptions outlined above.

When thermal hysteresis is neglected for case 1, Q' is greatly overestimated for both 252 K (Fig. 9(a)) and 278 K (Fig. 9(b)). The maximum difference in these instantaneous heat flux ratios is 51% at $Fo = 0.53$ in Fig. 9(b). The heat flux error introduced by neglecting hysteresis in adsorption and desorption for case 2 is much smaller, especially for a sub-freezing cold plate temperature (Fig. 9(a)). The maximum heat flux difference at $z = L$ for this case is 23% at $Fo = 0.2$ that is reduced to 6% at $Fo = 0.8$ for quasi-steady state (Fig. 9(b)).

To further demonstrate hysteresis effects, the rate of phase change, $\dot{m}$, at $z = L$ ($\dot{m} < 0$ means adsorption, condensation or ablimation and $\dot{m} > 0$ implies desorption, evaporation or sublimation) is presented for cases 1 and 2 in Figs. 10(a) and (b), respectively. Neglecting thermal hysteresis results in a different prediction of the mass accumulation and heat flux at

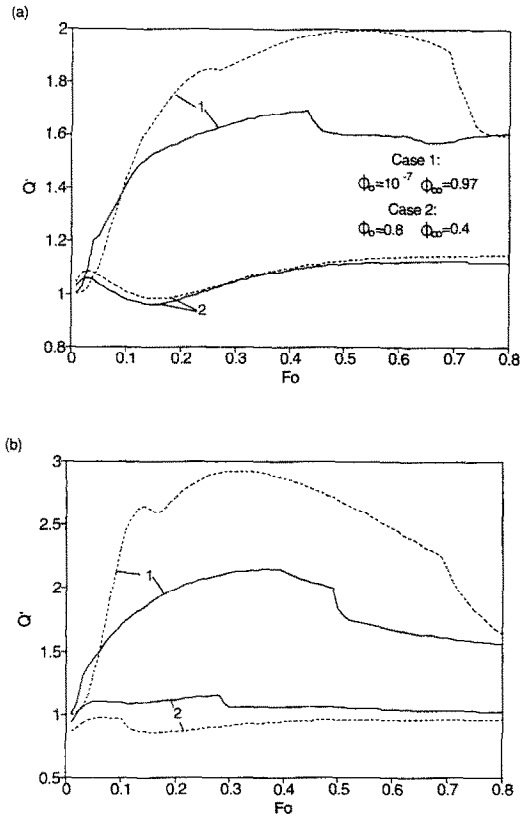

FIG. 9. Time variation of the heat-flux ratio for (a) $T_c = 252$ K and (b) $T_c = 278$ K. The broken lines correspond to the results assuming no thermal hysteresis effects.

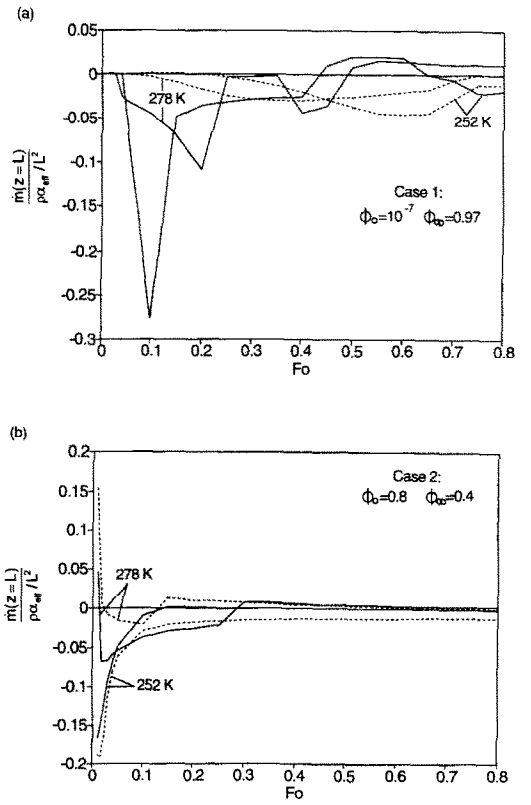

FIG. 10. Rate of phase change at the cold plate ($z = L$) for (a) case 1 and (b) case 2 at two different cold temperatures. The broken lines correspond to the results assuming no thermal hysteresis effects.

$z = L$. As shown in Fig. 10, the rate of phase change (dimensionless) at the cold plate, including thermal hysteresis effects, is very different from that neglecting thermal hysteresis. Because the heat flux at $z = L$ depends on the phase change at $z = L$ and throughout the insulation slab, the difference in the predicted $\dot{m}$ clearly explains the difference in Q' shown in Fig. 9.

7. CONCLUDING REMARKS

Thermal hysteresis has been defined by the differences between the adsorption and desorption isotherms and between heats of adsorption and desorption. New data are presented for the desorption process and are contrasted with previously obtained adsorption data. The significance of this phenomenon and its interaction with dynamic heat and mass transport processes such as that a building insulation undergoes are investigated through experiments and a numerical simulation. Based on the above discussion the following conclusions may be drawn within the scope of the present study:

(a) From the measurement of heat of desorption reported here and data for the heat of adsorption, the thermal hysteresis phenomenon clearly exists for typical commercial fiberglass insulation.

(b) During transient processes thermal hysteresis effects are pronounced regardless of whether the insulation slab is initially dry or wet and above or below the freezing temperature.

(c) Neglecting thermal hysteresis effects in simulating a dynamic transport process can lead to errors in the instantaneous heat flux of up to 51% for an initially dry fiberglass slab and 23% for an initially moist slab.

Acknowledgement—This study is partly supported through External Research Program from the Canadian Mortgage and Housing Corporation, which the authors owe a debt of graditude to.

REFERENCES

1. J. Lstiburek and J. Carmody, *Moisture Control Handbook*. Oak Ridge National Laboratory, ORNL/Sub/89-SD350/1 (1991).
2. H. S. Jhinger, G. K. Yuill and T. Hamlin, Comparison of a wall moisture model with field data, *Water in Exterior Building Walls*, ASTM STP **1107**, 105–123 (1991).
3. K. Vafai and H. C. Tien, A numerical investigation of phase change effects in porous materials, *Int. J. Heat Mass Transfer* **32**, 1261–1277 (1989).
4. Y.-X. Tao, R. W. Besant and K. S. Rezkallah, Unsteady heat and mass transfer with phase change in an insulation slab: frosting effects, *Int. J. Heat Mass Transfer* **34**, 1593–1603 (1991).
5. C. Langlais, M. Hyrien and S. Karlsfeld, Moisture migration in fibrous insulating material under the influence of a thermal gradient, *Moisture Migration in Buildings*, ASTM STP **779**, 191–206 (1982).
6. D. A. Pierce and S. M. Benner, Thermally induced hygroscopic mass transfer in a fibrous medium, *Int. J. Heat Mass Transfer* **29**, 1683–1694 (1986).
7. Y.-X. Tao, R. W. Besant and K. S. Rezkallah, The transient thermal response of a glass-fiber insulation slab with hygroscopicity effects, *Int. J. Heat Mass Transfer* **35**, 1155–1167 (1992).
8. H. C. Tien and K. Vafai, A synthesis of infiltration effects on an insulation matrix, *Int. J. Heat Mass Transfer* **33**, 1263–1280 (1990).
9. Y.-X. Tao, R. W. Besant and C. J. Simonson, Measurement of the heat of adsorption for a typical fibrous insulation, *ASHRAE Trans.* **98**(2), 495–501 (1992).
10. S. G. Gregg and K. S. Sing, *Adsorption, Surface Area and Porosity*, p. 17. Academic Press, London (1982).
11. K. Vafai and S. Sarkar, Condensation effects in a fibrous insulation slab, *J. Heat Transfer* **108**, 667–675 (1986).
12. K. Vafai and S. Whitaker, Simultaneous heat and mass transfer accompanied by phase change in porous insulation, *J. Heat Transfer* **108**, 132–140 (1986).
13. Y.-X. Tao, R. W. Besant and K. S. Rezkallah, Modelling of frost formation in a fibrous insulation slab and on an adjacent cold plate, *Int. Commun. Heat Mass Transfer* **18**, 609–618 (1991).

APPENDIX

The governing differential equations are:

β phase continuity equation:

$$\frac{\partial \varepsilon_\beta}{\partial t} + \frac{\dot{m}}{\rho_\beta} = 0 \tag{16}$$

Gas diffusion equation:

$$\frac{\partial(\varepsilon_v \rho_v)}{\partial t} - \dot{m} = \frac{\partial}{\partial z}\left(D_{\text{eff}} \frac{\partial \rho_v}{\partial z}\right) \tag{17}$$

Energy equation:

$$\rho c_p \frac{\partial T}{\partial t} + \dot{m}\Delta h = \frac{\partial}{\partial z}\left(k_{\text{eff}} \frac{\partial T}{\partial z}\right). \tag{18}$$

The algebraic equations of constraint are:

Volumetric constraint:

$$\varepsilon_\sigma + \varepsilon_\beta + \varepsilon_v = 1 \tag{19}$$

Thermodynamic relations:

$$p_a = p_t - p_v \tag{20}$$

$$p_a = R_a \rho_a T \tag{21}$$

$$p_v = R_v \rho_v T \tag{22}$$

$$p_v = p_0 \exp\left[-\frac{\Delta h}{R_v}\left(\frac{1}{T} - \frac{1}{T_{\text{ref}}}\right)\right] \tag{23}$$

where

$$\rho = \varepsilon_\sigma \rho_\sigma + \varepsilon_\beta \rho_\beta + \varepsilon_v(\rho_v + \rho_a) \tag{24}$$

$$c_p = \frac{\varepsilon_\sigma \rho_\sigma c_\sigma + \varepsilon_\beta \rho_\beta c_\beta + \varepsilon_v(c_v \rho_v + c_a \rho_a)}{\rho} \tag{25}$$

$$k_{\text{eff}} = \varepsilon_\sigma k_\sigma + \varepsilon_\beta k_\beta + \varepsilon_v \frac{k_v \rho_v + k_a \rho_a}{\rho_v + \rho_a}. \tag{26}$$

The boundary and initial conditions are:

$$k_{\text{eff}} \frac{\partial T(z=0,t)}{\partial z} = -h_a[T_\infty - T(z=0,t)], \tag{27}$$

$$D_{\text{eff}} \frac{\partial \rho_v(z=0,t)}{\partial z} = -h_m[\rho_\infty - \rho_v(z=0,t)], \tag{28}$$

$$T(z=L,t) = T_c, \tag{29}$$

$$\frac{\partial \rho_v(z = L, t)}{\partial z} = 0. \tag{30}$$

$\rho_v = \rho_s$, employing Clapeyron equation, will replace the above equation when $\rho_v(z = L, t)$ reaches the saturated value.

$$T(z, t = 0) = T_0, \tag{31}$$

$$\rho_v(z, t = 0) = \phi_0 \rho_s(T(z, t = 0)), \tag{32}$$

$$\varepsilon_\beta(z, t = 0) = \varepsilon_{\beta 0}(z). \tag{33}$$